Resonant multiple Andreev reflections in mesoscopic superconducting junctions

G. Johansson[1], E. N. Bratus[1,2], V.S. Shumeiko[1,2], and G. Wendin [1]

[1] *Department of Microelectronics and Nanoscience, Chalmers University of Technology and Göteborg University, S-412 96 Göteborg, Sweden*

[2] *B. Verkin Institute of Low Temperature Physics and Engineering, 310164 Kharkov, Ukraine*

(February 1, 2008)

We investigate the properties of subharmonic gap structure (SGS) in superconducting quantum contacts with normal-electron resonances. We find two distinct new features of the SGS in resonant junctions which distinguish them from non-resonant point contacts: (i) The odd-order structures on the current-voltage characteristics of resonant junctions are strongly enhanced and have pronounced peaks, while the even-order structures are suppressed, in the case of a normal electron resonance being close to the Fermi level. (ii) Tremendous current peaks develop at $eV = \pm 2E_0$ where E_0 indicates a distance of the resonance to the Fermi level. These properties are determined by the effect of narrowing of the resonance during multiple Andreev reflections and by overlap of electron and hole resonances.

I. INTRODUCTION

Resonant tunneling often plays an important role in current transport in transmissive superconducting junctions. The presence of impurities in the tunnel barriers may strongly affect Josephson tunneling[1–4] as well as Andreev transport under applied voltage[5,6] due to the resonant tunneling through localized impurity levels. A mechanism of resonant tunneling was assumed to be responsible for the unusual properties of junctions with disordered semiconducting barriers[7] and grain boundary Josephson junctions of high Tc materials[8]. Furthermore, in clean superconductor -semiconductor junctions, mobile electrons confined between the Schottky barriers form resonant states which determine specific properties of such junctions[9,10]. Similar resonant states are also important in recently fabricated ballistic superconductor-2D electron gas (2DEG) structures[11] where they are formed by the electron reflections by the gate potential. Moreover, the possibility to create quantum point contacts and quantum dots in such structures allows one to investigate quantum resonant transport through well resolved resonant levels[12]. Quantum resonant transport was also observed in metallic dots[13], and in contacts containing single wall nanotubes[14,15].

The properties of dc Josephson current in quantum resonant junctions as well as Andreev quantization have been discussed in various publications[16–19]. The subharmonic gap structure (SGS) in resonant junctions and the effect of the resonance on multiple Andreev reflections (MAR) is less investigated. Meanwhile, detailed theory of SGS in quantum point contacts[20–24] in combination with precise experiments on controllable break junctions[25,26] was found to be a powerful tool for investigation of intrinsic properties of the atomic-size contacts. Our preliminary results[27] have shown that SGS in resonant junction drastically differs from the SGS in non-resonant junction; similar results were obtained by different methods in Ref.[28]. In this paper, we present a detailed study of interplay of MAR with Breit-Wigner resonances in quantum junctions.

The structure of the paper is the following. In Section II we derive equations for the inelastic scattering amplitudes in resonant junctions. In Section III we discuss properties of the normal electron resonance in the proximity region between the superconducting electrodes. Results of numerical calculations of the current-voltage characteristic for different positions and widths of the resonance are presented in Section IV. Section V is devoted to perturbative analysis of resonant SGS.

II. SCATTERING AMPLITUDES.

We will consider a junction consisting of a ballistic normally conducting region separated from the superconducting electrodes by tunnel barriers, Fig. 1. The length of the junction L is assumed to be smaller than the coherence length, and therefore the distance between normal resonances will exceed the superconducting energy gap, $v_F/L > \Delta$ (v_F is the normal electron Fermi velocity, $\hbar = 1$). We will also assume that the resonances are well separated, $\Gamma \ll v_F/L$, where Γ is the resonance half-width, and that Coulomb charging effects do not dominate in the subgap voltage region, $E_C < 2\Delta$, where E_C is a Coulomb gap.

We will apply Landauer-Büttiker scattering theory[29–31] extended to superconducting junctions[21] for calculating the current. In voltage biased superconductive junctions, the quasiparticle scattering is inelastic due to time dependence of the superconducting phase difference across the junction, $\phi(t) = 2eVt$, and the scattering state wave functions consist of linear combinations of harmonics (sidebands) with energies $E_n = E + neV$ shifted by integer number of quanta eV with respect to the energy E of the incoming wave. Below we will consider one transport mode in the junction and choose the scattering state wave functions in the left (L) and right (R) electrodes having the form

$$\psi_L = e^{-iEt}\left[\delta_{j1}u_0^+ e^{ik_0^+ x} + \delta_{j2}u_0^- e^{-ik_0^- x}\right] + \sum_{n=-\infty}^{\infty} e^{-iE_n t}\left[a_n u_n^- e^{ik_n^- x} + c_n u_n^+ e^{-ik_n^+ x}\right] \quad (1a)$$

$$\psi_R = e^{i\sigma_z\phi(t)}\left\{e^{-iEt}\left[\delta_{j3}u_0^+ e^{-ik_0^+ x} + \delta_{j4}u_0^- e^{ik_0^- x}\right] + \sum_{n=-\infty}^{\infty} e^{-iE_n t}\left[b_n u_n^- e^{-ik_n^- x} + f_n u_n^+ e^{ik_n^+ x}\right]\right\}, \quad (1b)$$

where $u_n^\pm$ are (non-normalized) two-component elementary solutions of the Bogoliubov-de Gennes equations,

$$u_n^\pm = \frac{1}{\sqrt{2}}\begin{pmatrix} e^{\pm\gamma_n/2} \\ \sigma_n e^{\mp\gamma_n/2}\end{pmatrix}. \quad (2)$$

In this equation

$$e^{\gamma_n} = \frac{|E_n| + \xi_n}{\Delta}, \quad \xi_n = \begin{cases} \sqrt{E_n^2 - \Delta^2}, & |E_n| > \Delta \\ i\sigma_n\sqrt{\Delta^2 - E_n^2}, & |E_n| < \Delta \end{cases},$$

$$\sigma_n = \mathrm{sgn}(E_n), \quad k_n^\pm = \sqrt{2m(E_F \pm \sigma_n\xi_n)}.$$

Index $j = 1 - 4$ in Eqs. (1) labels scattering states of the electron- and hole-like quasiparticles incoming from the left ($j = 1, 2$) and right ($j = 3, 4$). The form of wave functions in Eqs. (1), (2) assumes that superconducting electrodes serve as equilibrium quasiparticle reservoirs, and that the potential difference between the reservoirs is absorbed into the time-dependent factor $e^{i\phi(t)}$ in Eq. (1b) due to appropriate choice of the gauge.

To match the wave functions in Eqs. (1) we will apply a transfer matrix technique. In the present case of an inelastic scattering problem, the connection between

ψ_L and ψ_R is non-local in time, and the corresponding transfer matrix $\mathbf{T}^S_{nm}$ mixes the sidebands,

$$\begin{pmatrix} A \\ B \end{pmatrix}_{Ln} = \sum_m \mathbf{T}^S_{nm} \begin{pmatrix} A \\ B \end{pmatrix}_{Rm}. \tag{3}$$

The matrix $\mathbf{T}^S_{nm}$ is a 4×4 matrix defined on a space of wave function coefficients, $A = (A^+, A^-)$, $B = (B^+, B^-)$,

$$\psi_n = e^{-iE_n t}\Big[A^+_n u^+_n e^{ik^+_n x} + A^-_n u^+_n e^{-ik^+_n x} + B^+_n u^-_n e^{ik^-_n x} + B^-_n u^-_n e^{-ik^-_n x}\Big]. \tag{4}$$

The transfer matrix in Eq. (3) can be expressed, similarly to the case of unbiased junctions[19], through a transfer matrix $T(E)$ associated with elastic electron scattering by the normal junction. Let us introduce auxiliary normal regions between the superconductors and the junction, the length of which normal regions will be put equal to zero at the end of the calculations. The wave function in the normal region has the form

$$\psi^N_n = \begin{pmatrix} A^{N+}_n e^{ik^{N+}_n x} + A^{N-}_n e^{-ik^{N+}_n x} \\ B^{N+}_n e^{ik^{N-}_n x} + B^{N-}_n e^{-ik^{N-}_n x} \end{pmatrix} e^{-iE_n t}, \tag{5}$$

where $k^{N\pm}_n = \sqrt{2m(E_F \pm E_n)}$ is the normal electron wave vector. The wave functions Eq. (5) in the left and right normal regions are related as

$$\begin{pmatrix} A^N \\ B^N \end{pmatrix}_{Ln} = \mathbf{T}^N_n \begin{pmatrix} A^N \\ B^N \end{pmatrix}_{Rn}, \quad \mathbf{T}^N_n = \begin{pmatrix} T(E_n) & 0 \\ 0 & T(-E_n) \end{pmatrix}. \tag{6}$$

We note that the transfer matrix $T(E)$ describes scattering of the normal electrons by the actual potential of the junctions at a given voltage, i.e. it includes effects of potential deformation due to applied voltage, $T(E;V)$.

Continuous matching at the left SN interface yields in quasiclassical approximation $k_n \approx k^N_n \approx k_F$,

$$\begin{pmatrix} A^N \\ B^N \end{pmatrix}_{Ln} = \mathbf{T}^{NS}_n \begin{pmatrix} A \\ B \end{pmatrix}_{Ln}, \quad \mathbf{T}^{NS}_n = \begin{pmatrix} e^{\gamma_n/2} & e^{-\gamma_n/2} \\ \sigma_n e^{-\gamma_n/2} & \sigma_n e^{\gamma_n/2} \end{pmatrix}. \tag{7}$$

A matching condition at the right NS interface is derived in a similar way but an additional time-dependent factor $e^{i\sigma_z eVt}$ in Eq. (1b) must be taken into account. The latter gives different equations for upper (electron) and lower (hole) components of the coefficient vectors:

$$A^N_{Rn} = \mathbf{P}^+ \mathbf{T}^{NS}_{n+1} \begin{pmatrix} A \\ B \end{pmatrix}_{R(n+1)}, \quad B^N_{Rn} = \mathbf{P}^- \mathbf{T}^{NS}_{n-1} \begin{pmatrix} A \\ B \end{pmatrix}_{R(n-1)}. \tag{8}$$

In this equation, $\mathbf{P}^\pm$ are projectors on upper/lower vector components.

Combination of Eqs. (6)-(8) gives the following equation for the transfer matrix in Eq. (3)

$$\mathbf{T}^S_{nm} = \sum_\pm (\mathbf{T}^{NS}_n)^{-1} \mathbf{T}^N_n \mathbf{P}^\pm \mathbf{T}^{NS}_m \delta_{m(n\pm1)}. \tag{9}$$

Normal electron transfer matrix enters this equation with different arguments $\pm E_n$. This energy difference introduces effects of electron-hole dephasing during quasiparticle propagation through the junction. In non-resonant short constrictions, the energy dispersion of the transfer matrix is negligible, and equation (9) is equivalent to the matching equation derived in Ref.[21]. In resonant junctions (and also in long SNS and SIS junctions[32]) dephasing effects are important.

The matching equations (3),and (9) can be written in an equivalent form,

$$\mathbf{P}^\pm \mathbf{T}^{NS}_n \begin{pmatrix} A \\ B \end{pmatrix}_{Ln} = T(\pm E_n) \mathbf{P}^\pm \mathbf{T}^{NS}_{Rn\pm1} \begin{pmatrix} A \\ B \end{pmatrix}_{R(n\pm1)}. \tag{10}$$

Applied to the scattering state wave functions in Eqs. (1), it yields the following recurrences for the scattering amplitudes:

$$e^{\sigma_z\gamma/2}\delta_{n0}\begin{pmatrix}\delta_{j1}\\ \delta_{j2}\end{pmatrix} + e^{-\sigma_z\gamma_n/2}\begin{pmatrix}a\\ c\end{pmatrix}_n = T(E_n)\left[e^{\sigma_z\gamma/2}\delta_{(n+1)0}\begin{pmatrix}\delta_{j3}\\ \delta_{j4}\end{pmatrix} + e^{-\sigma_z\gamma_{n+1}/2}\begin{pmatrix}f\\ b\end{pmatrix}_{n+1}\right] \tag{11a}$$

$$e^{-\sigma_z\gamma/2}\delta_{n0}\begin{pmatrix}\delta_{j1}\\ \delta_{j2}\end{pmatrix} + e^{\sigma_z\gamma_n/2}\begin{pmatrix}a\\ c\end{pmatrix}_n = T(-E_n)\sigma_n\sigma_{n-1}\left[e^{-\sigma_z\gamma/2}\delta_{(n-1)0}\begin{pmatrix}\delta_{j3}\\ \delta_{j4}\end{pmatrix} + e^{\sigma_z\gamma_{n-1}/2}\begin{pmatrix}f\\ b\end{pmatrix}_{n-1}\right]. \tag{11b}$$

Analytical solutions of the recurrences in Eqs. (11) can be presented in chain-fraction form (see Appendix A) similar to the case of non-resonant junctions[20,21].

III. MODEL FOR RESONANCE.

Now we will specify the transfer matrix for the resonant junction. We will restrict ourselves to symmetric junctions, $T_{11} = T^*_{22} = 1/d$ and $T_{21} = T^*_{12} = r/d$ and assume the Breit-Wigner resonance form for transmission and reflection amplitudes d and r respectively,

$$d(E) = \frac{i\Gamma}{E - E_r + i\Gamma}, \quad r(E) = -\frac{E - E_r}{E - E_r + i\Gamma}. \tag{12}$$

The position of the resonance level E_r as well as the resonance half-width Γ are generally dependent on the applied voltage. However, while the subharmonic gap structure is affected in an essential way by the position of the resonance, the dependence on the resonance width is less important. Thus we will assume $\Gamma = const$. We will not specify the voltage dependence of resonance level position, but rather present the current as a function of two variables: driving voltage and resonance position, $I(V, E_r)$. The current voltage characteristics can then be

reconstructed from such a dependence by specifying the $E_r(V)$ dependence determined by self-consistent distribution of the electric potential across the junction.

The normal electron resonance, being confined between superconducting electrodes, possesses specific properties which will be important for further analysis of the resonant MAR. Since the transfer matrix $T(E)$ enters the recurrences for the scattering amplitudes in Eq. (11) at two different energies $\pm E$, the proximity resonance consists of two, electron and hole, resonances situated symmetrically with respect to the Fermi level, $E = \pm E_r$. Within the adopted approach, the current is calculated by using the scattering amplitudes defined in the *superconducting electrodes* [see further Eq. (15)] and the recurrences in Eq. (11) are formulated for these amplitudes. Although equivalent, such an approach is different from the discussion of MAR amplitudes in the normal region of the junction (see, e.g.[36]). Within our approach, the non-superconducting region of the junction is considered as a black box and is represented by the transfer matrix $T(E)$. Due to the different choices of gauge in the left and right electrodes, the resonance is seen from the left and right electrodes at different energies [cf. Eqs. (7) and (8)]. Indeed, the resonances are seen from the left electrode at $E = \pm E_r$, i.e. quasiparticles incoming from the left undergo resonant transition if $E = \pm E_r$, while the resonances are seen from the right electrode at $E = \pm(E_r + eV)$, as shown in Fig. 2. In the scattering diagram in Fig. 2c, the resonance therefore is presented with two segments: $E_n = E_r \leftrightarrow E_{n+1} = E_r + eV$ for the electron resonance, and $E_n = -E_r \leftrightarrow E_{n-1} = -E_r - eV$ for the hole resonance.

There is a symmetry between the scattering states originating from the left and right electrodes:

$$\begin{pmatrix} a \\ c \end{pmatrix}_{n,3} (\gamma, \Gamma, E_0) = \sigma_0 \sigma_n \begin{pmatrix} f \\ b \end{pmatrix}_{n,1} (-\gamma, -\Gamma, -E_0), \quad (13)$$

with an analogous relation for the second pair of scattering amplitudes. In Eq. (13), $E_0 = E_r + eV/2$ is the distance of the normal resonance level with respect to the midpoint between the chemical potentials in the left and right electrodes. Equation (13) leads to a symmetry property of the current which is an even function of the resonance position E_0: $I(V, E_0) = I(V, -E_0)$. Below we will indicate the resonance position by means of the energy E_0 and abbreviate the Breit-Wigner amplitudes (12),

$$d_n^{\pm} = \frac{i\Gamma}{E_n^{\pm} + i\Gamma}, \;\; r_n^{\pm} = \frac{E_n^{\pm}}{E_n^{\pm} + i\Gamma}, \quad E_n^{\pm} = E_n \mp (E_0 - eV/2). \quad (14)$$

IV. DC CURRENT.

In the quasiclassical approximation, the equation for the current reads[20,21]

$$I = \frac{e\Delta}{2\pi} \int_{\Delta}^{\infty} \frac{dE}{\xi} \sum_{n=odd} \cosh(Re\gamma_n) \tanh\frac{E}{2T} \left[\sum_{j=1,2} \left(|b_{n,j}|^2 - |f_{n,j}|^2 \right) - \sum_{j=3,4} \left(|c_{n,j}|^2 - |a_{n,j}|^2 \right) \right] \quad (15)$$

The current in Eq. (15) is calculated using transmitted states (in the right and left electrodes for scattering states $j = 1, 2$ and $j = 3, 4$ respectively), and it consists of contributions from all odd sidebands. By virtue of the symmetry equations

$$\begin{pmatrix} f \\ b \end{pmatrix}_{n,2} (\gamma, T) = \begin{pmatrix} b \\ f \end{pmatrix}_{n,1} (-\gamma, T^*),$$
$$\begin{pmatrix} a \\ c \end{pmatrix}_{n,2} (\gamma, T) = \begin{pmatrix} c \\ a \end{pmatrix}_{n,1} (-\gamma, T^*), \quad (16)$$

directly following from Eqs. (11) (analogous relations hold for the scattering states $j = 3, 4$) and symmetry equations (13), the current in Eq. (15) can be expressed through the sideband contributions

$$K_n = \left[|b_n|^2 - |f_n|^2 \right] \cosh(Re\gamma_n) \quad (17)$$

of one single scattering state ($j = 1$, index j is omitted),

$$I = \frac{e\Delta}{2\pi} \int_{\Delta}^{\infty} \frac{dE}{\xi} \sum_{n=odd} \left[K_n - \bar{K}_n + (E_0 \to -E_0) \right] \tanh\frac{E}{2T}, \quad (18)$$

where $\bar{K}_n = K_n(-\xi_n, -\Gamma)$.

Equation Eq. (18) together with the recurrences in Eqs. (11) provide a basis for numerical calculation of the current. The calculation of scattering amplitudes should obey the boundary condition at $\pm$ infinity where the amplitudes approach zero. The simplest way to obtain such solutions is to iterate the recurrences from large $|E_n|$ towards E. The correct solution will then grow exponentially and numerically "kill" the solution growing at infinity. By this procedure one gets the correct scattering states for each incoming quasiparticle at every energy.

The results of numerical calculation of current-voltage characteristics (IVC) are presented in Fig. 3 for different values of resonance level position $E_0 = const$. This particular case corresponds to a perfectly symmetric distribution of the electric potential across the junction with E_0 indicating the departure of the resonance level from the Fermi level in equilibrium ($V = 0$). The IVC with the resonance level situated at the Fermi level, $E_0 = 0$, shows an onset of the single-particle current at $eV = 2\Delta$ accompanied by a current peak caused by large density of states near the superconducting gap [see below Eqs. (24-25)]. Such behaviour of the single-particle current has been observed in the experiments on metallic dots[13] and carbon-nanotube junctions[33]. A striking feature of this IVC is the absence of current structure at $eV = \Delta$, while the structure at $eV = 2\Delta/3$ is pronounced, consisting of a peak similar to the structure of the single-particle current. Calculation of the IVC at lower voltage, presented

in Fig. 4, shows the same feature - only odd subharmonic gap structures are present.

If the resonant level departs from the Fermi level and $E_0 \neq 0$, the single-particle current onset shifts towards larger voltage, $eV > 2\Delta$, and the current peak broadens. A striking feature in this case is the development of a huge current peak at voltages lower than the position of the structure of single-particle current. This peak, associated with resonant pair current (see below Sec. V), appears as soon as $E_0 > \Delta/2$ and is situated at voltage $eV = 2E_0$ which coincides with position of the resonant current onset in normal junctions. If the resonance level departs far from the Fermi level, $E_0 \gg \Delta$, the IVCs in the subgap voltage region $eV < 2\Delta$ approach the form typical for non-resonant point contacts, as could be expected, while a broadening of the resonance, $\Gamma \gg \Delta$, gives rise to SNS-type IVCs, as shown in Fig. 5.

A complete description of the current in resonant junctions is given by the function $I(V, E_0)$, as already mentioned in Section III. A plot of this function is presented in Fig. 6. The IVCs plotted in Figs. 3-5 correspond to horizontal cuts ($E_0 = const$) of the plot in Fig. 6. In Fig. 6a, the light wedge-like region at $eV > 2\Delta$ corresponds to the resonance single-particle current. The resonant peak of the pair current is seen as the light streaks directed along the lines $E_0 = \pm eV/2$, the structure starts at $eV = \Delta$. Fig. 6b presents a similar plot for the region of small voltage, $eV < \Delta$. The picture shows quite complex structure of the current consisting of wedge-like plateaux of the resonant current as well as of light streaks corresponding to current peaks.

In order to interpret the features of the IVCs one needs to analyze the properties of the side-band currents K_n presented in Eqs. (17) and (A7).

V. DISCUSSION

A convenient expression for analysis of the subharmonic gap structure is derived in Appendix B:

$$I_{SGS}(V, E_0) = \sum_{n=1}^{\infty} I_n(V, E_0),$$

$$I_n(V, E_0) = \frac{e\Delta}{2\pi} \int_{\Delta}^{neV-\Delta} \tanh \frac{E}{2T} \frac{dE}{\xi} \left[\tilde{K}_{-n} - \tilde{\bar{K}}_{-n} + (E_0 \to -E_0) \right] \qquad (19)$$

In Eq. (19) only contributions of processes of creation of real excitations (transitions across the gap $E > \Delta \to E_n < -\Delta$) are retained which are responsible for the subharmonic gap structure[21] while a contribution of thermal excitations is omitted. Furthermore, the sum over the sideband currents in Eq. (18) is now rearranged in order to explicitly separate the contributions of all inelastic channels [contributions of *even* inelastic channels are hidden in Eq. (18)]. This is done by proper renormalization of the sideband currents $K_n \to \tilde{K}_n$ presented in Appendix B, the equation for $\tilde{K}_n$ being given in Eq. (B9). We will now develop a perturbative analysis of the current in the limit of small width of the resonance, $\Gamma \ll \Delta$, and zero temperature.

A. Single-particle current

The single-particle current is given by the first term in Eq. (19). In accordance with Eq. (B9), it has explicit form

$$I_1 = \frac{4e}{\pi} \int_{\Delta}^{eV-\Delta} dE \, \frac{|E_{-1}| \xi \xi_{-1}}{\Delta^3} \left\{ D_0^- \left(\frac{e^{-\gamma}}{P_1} + \frac{e^{\gamma}}{\bar{P}_1} \right) + (E_0 \to -E_0) \right\}, \qquad (20)$$

P_1 is defined in Eq. (B10). This current has no contribution from Andreev reflections and it has only one resonance. It is sufficient to consider only scattering states incoming from the left [the first term in curly brackets in Eq. (20)], the resonance equation in this case being $E_0^- = 0$. The resonance is only involved if it belongs to the integration interval. This determines the resonance region $eV/2 > \Delta + |E_0|$ in the plane (V, E_0) (region I in Fig. 7). The resonant scattering diagram is shown in Fig. 8a.

In non-resonant junctions, the currents $\tilde{K}_{-n}$ in Eq. (19) have the singularities which are responsible for the current onset at $eV = 2\Delta$ and subharmonic gap structure. In resonant junctions, the singularities are washed out due to strong electron-hole dephasing and the resonant transmissivity is simultaneously renormalized. In the case of a single-particle current in Eq. (20), the onset of non-resonant current is caused by zeros of the function P_1. Calculation of P_1 for the resonant junctions by using the rule in Eq. (B10) and retaining only the resonant scattering amplitude d_0^- yields

$$\frac{D_0^-}{P_1} \approx \frac{\Delta^4 \Gamma^2}{16 \xi^2 \xi_{-1}^2} \left| E_0^- + \frac{i}{2} \left(\Gamma_0 + \Gamma_{-1} \right) \right|^{-2}, \qquad (21)$$

where $\Gamma_n = \Gamma |E_n| / \xi_n$. Equation (21) shows the transformation of the resonant tunneling probability in the superconducting junctions: the resonance width is broadened due to superconducting density of states E/ξ. Taking into account Eq. (21) and similar equations for the other terms in Eq. (20), we present the single-particle current on the form of the Landauer formula,

$$I_1 = \frac{e}{\pi} \int_{\Delta}^{eV-\Delta} dE \, \tilde{D}_1(E), \qquad (22)$$

with the effective single-particle transmission coefficient,

$$\tilde{D}_1(E) = \frac{\Gamma_0 \Gamma_{-1}}{|E_0^- + (i/2)(\Gamma_0 + \Gamma_{-1})|^2}. \qquad (23)$$

Similar equation have been derived in Ref.[28] using a different method.

Equations (22) and (23) determine the current in the wedge region in Fig. 6a. In the limit of $\Gamma \to 0$, the resonant current reads

$$I_1 = \frac{2e^2\Gamma V_+ V_- \theta[eV - 2(\Delta + |E_0|)]}{V_-\sqrt{(eV_+)^2 - 4\Delta^2} + V_+\sqrt{(eV_-)^2 - 4\Delta^2}}, \quad (24)$$

where $eV_\pm = eV \pm 2|E_0|$. This equation quantitatively describes the single-particle current feature in Fig. 3. The current has maximum at the wedge edges and decreases at large eV approaching the value for the resonant current in the normal junction $I_N = e\Gamma$ (see Fig. 3),

$$I_1 = I_N \begin{cases} \dfrac{2|E_0| + \Delta}{\sqrt{|E_0|(|E_0| + \Delta)}}, & eV = 2(\Delta + |E_0|) \\ 1 + \dfrac{2\Delta^2}{(eV)^2}, & eV \gg \Delta, E_0 \end{cases} \quad (25)$$

The current peak is the result of enhancement of the effective width of the resonance in Eq. (23) at low energy $\xi = 0$ Equation (25) is everywhere applicable except of the wedge vertex, $E_0 = 0$, $eV = 2\Delta$, where the current grows without limit. In fact, the current consists of the peak and turns to zero at $eV = 2\Delta$ due to shrinking of interval of integration in Eq. (22) in this region. The maximum current is achieved when the integration interval becomes comparable with the resonance width, $eV - 2\Delta \sim \Gamma\sqrt{\Delta/(eV - 2\Delta)}$. These arguments yield estimate for the maximum current at $eV = 2\Delta$, $(I_1)_{max} \sim I_N(\Delta/\Gamma)^{1/3}$.

B. Pair current

The pair current has form

$$I_2 = \frac{4e}{\pi}\int_\Delta^{2eV-\Delta} dE\, \frac{|E_{-2}|\xi\xi_{-2}}{\Delta^3}$$
$$\left\{ D_0^- D_{-2}^+ \left(\frac{e^{-\gamma}\varphi_{-2}}{P_2} + \frac{e^{\gamma}\bar{\varphi}_{-2}}{\bar{P}_2} \right) + (E_0 \to -E_0) \right\}. \quad (26)$$

Restricting again the consideration with quasiparticles incoming from the left, we find that this current is contributed by two resonances, $E_0^- = 0$ and $E_{-2}^+ = 0$, which simultaneously enter the integration interval within the region II_1 in Fig. 7 (region II_2 corresponds to resonant quasiparticles incoming from the right). Therefore, the resonant pair current only appears if the normal resonance is sufficiently far from the Fermi level, $E_0 > \Delta/2$, while at $E_0 < \Delta/2$ the current is non-resonant within the voltage interval $\Delta < eV < 2\Delta$. This means in particular that the onset of the pair current at $eV = \Delta$ is small: $I_2 \sim I_N(\Gamma/\Delta)^3$ if $E_0 = 0$. In regions II, the pair current undergoes resonant enhancement, $I_2 \sim I_N(\Gamma/\Delta)^2$ due to independent contributions of two separate resonances (Fig. 8b), each contribution being described by the equations similar to Eqs. (22), (23).

The most interesting phenomenon in the resonant pair current is the overlap of the resonances occurring along the lines $eV = \pm 2|E_0|$ in Fig. 7. The overlap of the resonances produces a huge current peak near these lines (seen as light streaks in the Fig 6a; we note that these lines correspond to the position of the onset of resonant current in normal junctions). The scattering diagram for this case is presented in Fig. 8c. Applying Eq. (B10) for calculation of P_2 and retaining both the resonant amplitudes d_0^- and d_{-2}^+, we obtain

$$\frac{D_0^- D_{-2}^+}{P_2} \approx \frac{\Delta^6\Gamma^4}{|8\xi\xi_{-1}\xi_{-2}|^2} \left| \left[E_0^- + i\left(\frac{\Gamma_0 + \Gamma_{-1}}{2} \right) \right] \right.$$
$$\left. \left[E_{-2}^+ + i\left(\frac{\Gamma_{-1} + \Gamma_{-2}}{2} \right) \right] - \frac{\Gamma^2\Delta^2}{4|\xi - 1|^2} \right|^{-2}. \quad (27)$$

Substituting Eq. (27) into Eq. (26) for the current and collecting the contributions of all scattering modes, we find

$$I_2 = \frac{e}{\pi}\int_\Delta^{2eV-\Delta} dE\, \tilde{D}_2(E), \quad (28)$$

where

$$\tilde{D}_2(E) = \frac{\Gamma_0\Gamma_{-2}\Gamma^2\Delta^2/4|\xi_{-1}|^2}{|\tilde{E}_0^-\tilde{E}_{-2}^+ - (\Gamma_0\Gamma_{-2} + \Gamma^2\Delta^2/|\xi_{-1}|^2)/4 + i(\Gamma_{-2}E_0^- + \Gamma_0 E_{-2}^+)/2|^2}$$
$$\tilde{E} = E + i\Gamma_{-1}/2. \quad (29)$$

Equation (29) shows a remarkable similarity to the resonant transmissivity of Schrödinger three-barrier structures: the probability to leak outside the superconducting gap through the sidebands $n = 0$ and $n = -2$ (Fig. 8c) corresponding to probability of tunneling through side barriers, while the probability of Andreev reflection by the sideband $n = -1$ corresponding to transmissivity of a central barrier. Such three-barrier structures have been investigated, e.g. in connection with normal electron transport properties of coupled quantum dots[34,35]. The strong overlap of the resonances is explained by the fact that shift of the resonances is proportional to Γ^2 due to Andreev reflection, according to Eq. (29), while the resonance width is proportional to the first power of Γ (the quantity Γ_{-1} is equal to zero at the lines $eV = \pm 2|E_0|$).

In the vicinity of the lines $eV = \pm 2|E_0|$ and in the limit $\Gamma \to 0$, the pair current has following form

$$I_2 = I_N \frac{\Gamma^2 eV\sqrt{(eV)^2 - \Delta^2}}{(eV - 2|E_0|)^2[(eV)^2 - \Delta^2] + \Gamma^2[2(eV)^2 - \Delta^2]}. \quad (30)$$

(We notice that this formula is valid at all voltages $eV > \Delta$ because the side band $n = -1$ is inside the energy gap if $eV \approx \pm 2|E_0|$). Equation (30) describes the current peak in Fig. 3, the height of the peak

$$(I_2)_{max} = I_N \, \frac{2|E_0|\sqrt{4E_0^2 - \Delta^2}}{8E_0^2 - \Delta^2} \tag{31}$$

being comparable to the magnitude of the resonant single-particle current, in particular, $(I_2)_{max} = I_N/2$ at $E_0 \gg \Delta$.

According to Eq. (30) the resonant pair current tends to zero at large voltage $eV \gg \Delta, E_0$, which means that, rigorously speaking, there is no resonant excess current. However, if the resonance is far beyond the gap, $|E_0| \gg \Delta$, the current may strongly deviate from the current in the normal junction in the region $\Delta \ll eV \ll 2|E_0|$ because the single-particle current is non-resonant in this region, while the pair current is resonant. Such an effect is particularly pronounced in the junctions where the resonance level follows the chemical potential of one of the electrodes, $E_0(eV) \pm eV/2 \approx \epsilon = const$. The IVC in this case corresponds to cuts in the plot in Fig 6a parallel to the light streaks. In such a case, the peak of the pair current is very broad, and even transforms into a plateau with a sharp onset at $eV = \Delta$ ($\epsilon = 0$), as shown in the inset in Fig. 10. The magnitude of the current at the plateau can be found directly from Eq. (A7) when assuming $E_0 = \epsilon \pm eV/2$ and $eV = \infty$,

$$I_2(\epsilon, \Gamma) = \frac{2e}{\pi} \int_0^\infty dE \, \cosh(Re\gamma) \\ \frac{2D_0^- \sinh(Re\gamma) + D_0^- D_0^+ e^{-Re\gamma}}{|e^\gamma - r_0^{-*} r_0^+ e^{-\gamma}|^2}, \tag{32}$$

$D_0^\pm = \Gamma^2/[((E \mp \epsilon)^2 + \Gamma^2]$. This current as function of ϵ is shown in Fig. 10.

There is an interesting difference between the property of the resonance in the single-particle current and that of individual resonances of the pair current. To be specific, let us consider the resonance E_0^-: in the pair current this resonance is more narrow because the quantity Γ_{-1} is imaginary and causes a resonant shift rather than a contribution to the resonance width. The physical reason for this squeezing of the resonance is that direct leakage of a quasiparticle through the side band $n = -1$ is blocked, and the only escape from the resonant region into the continuum is through the states of the side band $n = 0$.

C. High-order currents

The effect of the resonance narrowing is even more important for the third order current,

$$I_3 = \frac{4e\Delta}{\pi} \int_\Delta^{3eV-\Delta} dE \, \frac{|E_{-3}|\xi\xi_{-3}}{\Delta^3} \\ \left\{ D_0^- D_{-2}^+ D_{-2}^- \left(\frac{e^{-\gamma}\varphi_{-3}}{P_3} + \frac{e^{\gamma}\bar{\varphi}_{-3}}{\bar{P}_3} \right) + (E_0 \to -E_0) \right\}. \tag{33}$$

The third order current has three resonances at $E_0^-, E_{-2}^+, E_{-2}^- = 0$ which belong to the interval of integration within the regions III_1, III_2, III_3 in Fig. 7, respectively. The side resonances at $E_0^-, E_{-2}^- = 0$ are characterized by an effective transmissivity similar to the effective transmissivity of the resonances of pair current (times additional factor $\sim \Gamma^2$). The contribution of these resonances in the current is therefore estimated as $I_3 \sim I_N(\Gamma/\Delta)^4$. The central resonance $E_{-2}^+ = 0$ is much more narrow. Indeed, in this case (Fig. 8d), direct leakage of the resonant particle into continuum is blocked at the both sidebands $n = -1, -2$, and the particle can escape only through the sideband states $n = 0, -3$, traversing the junction one more time. The central resonance determines the current in the vicinity of the threshold $eV = 2\Delta/3$, $E_0 = 0$.

Calculation of the quantity P_3 in region III_2 according to Eq. (B10) yields

$$\frac{D_0^- D_{-2}^+ D_{-2}^-}{P_3} \approx \frac{\Delta^4 \tilde{\Gamma}_0 \tilde{\Gamma}_{-3}}{|4^2 \xi\xi_{-3} E E_{-3}|} \left| \tilde{E}_{-2}^+ + \frac{i}{2} \left(\tilde{\Gamma}_0 + \tilde{\Gamma}_{-3} \right) \right|^{-2} \tag{34}$$

where $\tilde{E}_{-2}^+ = E_{-2}^+ + i(\Gamma_{-1} + \Gamma_{-2})/2 + O(\Gamma^2)$ and $\tilde{\Gamma}_0 = \Gamma_0 D_0^- \Delta^2/4|\xi|^2$, $\tilde{\Gamma}_{-3} = \Gamma_{-3} D_{-2}^- \Delta^2/4|\xi_{-2}|^2$. According to Eq. (34), the resonance width is of the order of $\tilde{\Gamma} \sim \Gamma^3$ which yields giant enhancement of the current $I_3 \sim I_N(\Gamma/\Delta)^2$, exceeding by two orders of Γ the contribution of the side resonances. Such narrowing of the central resonance occurs in the quadrangle region in Fig. 7 bounded by the edges of the resonance region III_2 and regions II. The current in this region has a form similar to the one in equation (22),

$$I_3 = \frac{e}{\pi} \int_\Delta^{3eV-\Delta} dE \, \tilde{D}_3(E), \tag{35}$$

with the effective resonant transmissivity

$$\tilde{D}_3(E) = \frac{3\tilde{\Gamma}_0 \tilde{\Gamma}_{-3}}{\left| \tilde{E}_{-2}^+ - i \left(\tilde{\Gamma}_0 + \tilde{\Gamma}_{-3} \right)/2 \right|^2}. \tag{36}$$

In the limit of small $\Gamma \to 0$, the current reads

$$I_3 = 6e\tilde{\Gamma}_0 \tilde{\Gamma}_{-3} / \left(\tilde{\Gamma}_0 + \tilde{\Gamma}_{-3} \right)_{E=|E_0|+3eV/2}. \tag{37}$$

The phenomenon of resonance narrowing provides the explanation for the absence of current structure at voltage $eV = \Delta$, namely the dominance of the third order current I_3 at the threshold of the pair current. The current in Eq. (37) is responsible for the light wedge-like region at $eV < \Delta$ in Fig. 6b. Similarly to the case of single-particle current, the third-order current in Eq. (37) has a peak at the edges of the wedge with the height increasing proportionally to $(eV - 2\Delta/3)^{-1/2}$ towards the vertex of the wedge, $eV = 2\Delta/3$, $E_0 = 0$. This growth is again limited due to interplay between shrinking integration interval and growing resonance width, $eV - 2\Delta/3 \sim \Gamma^3[\Delta/(eV - 2\Delta/3)]^{1/2}$. This estimate

gives a height $(I_3)_{max} \sim I_N(\Gamma/\Delta)$ of the current peak at $eV = 2\Delta/3$. As one may see in Fig. 6b, there are no current structures at the edges $eV = 2(\Delta - |E_0|)$ of the above mentioned quadrangle where the the narrow resonance of three-particle current dies: this is because of the resonant pair current emerges at the same lines, giving rise to a gradual cross over between three-particle current and pair current both having the magnitude of the order of $I_N(\Gamma/\Delta)^2$.

The phenomenon of resonance narrowing results in enhancement of central resonances in all higher odd-order currents, giving rise to the current peaks at $eV = 2\Delta/(2k+1)$, $E_0 = 0$ with the height $I_{max} \sim I_N(\Gamma/\Delta)^{2k-1}$. The magnitude of the current between neighbouring peaks is $I \sim I_N(\Gamma/\Delta)^{2k}$. Also, the overlap of narrow resonances of the even-order currents near the lines $eV = \pm 2|E_0|$ yields current peaks with the height $I \sim I_N(\Gamma/\Delta)^{2k}$ within the intervals $2\Delta/(2k+2) < eV < 2\Delta/2k$. These current peaks are clearly seen in Fig. 6b in the form of light streaks.

VI. CONCLUSION.

In conclusion, we have considered effect of the normal electron resonant tunneling on the subharmonic gap structure (SGS) in mesoscopic superconducting junctions. In non-resonant tunnel junctions, the SGS consists of sharp onsets and narrow peaks of the current at voltage $eV = 2\Delta/n$. In resonant junctions, SGS is considerably modified depending on the position of resonance level with respect to the chemical potentials of the electrodes. If the resonance level is situated exactly in the middle between the chemical potentials of electrodes, the odd-n current structures are tremendously enhanced while the even-n current structures are not affected by the resonance. This enhancement is explained by narrowing of the resonance during multiple Andreev reflections. When the resonance departs from the midpoint between the chemical potentials of electrodes, new current structures appear at $eV = \pm 2E_0$ in a form of current peaks. This feature results from overlap of electron and hole resonances.

In our calculations, the Coulomb charging energy was assumed to be smaller than the superconducting gap, and the charging effects were neglected. In experiments on metallic dots[13] and carbon nanotubes[14,15,33], the opposite situation has been observed with the Coulomb charging energy exceeding the superconducting gap which led to suppression of the subgap current. The charging energy in quantum transport experiments can be reduced by enhancing capacitance of the resonant structure, e.g. by using substrates with large dielectric constants. This will allow direct application of our results to such structures. Another way would be to use high-T_c materials for fabrication of superconducting electrodes for the nanotube experiments. Our theory is applicable to ballistic plane junctions with large capacitance such as resonant junctions in high mobility S-2DEG-S devices and atomic plane junctions in layered cuprates (intrinsic Josephson junctions[37]). Current-voltage characteristics of such multimode junctions can be obtained on the basis of our theory by summation of contributions of all transport modes.

VII. ACKNOWLEDGEMENT

This work has been supported by the Swedish Natural Science Research Council (NFR), the Swedish Board for Technical Development (NUTEK), the Swedish Royal Academy of Sciences (KVA), and the New Energy Development Organization (NEDO), Japan.

APPENDIX A: DERIVATION OF CURRENT

Following the method of Ref.[20,21], we eliminate the Andreev scattering amplitudes a_n and b_n from Eqs. (11) for the scattering state $j = 1$ and obtain a closed set of equations for the normal amplitudes c_n and f_n,

$$c_{2n} + V^-_{2n+1} f_{2n+1} + V^+_{2n-1} f_{2n-1} = \frac{2\xi}{\Delta \Xi_0}\delta_{n0} \qquad \text{(A1)}$$

$$f_{2n+1} + V^+_{2n+2} c_{2n+2} + V^-_{2n} c_{2n} = 0.$$

The coefficients in these equations are

$$\begin{aligned} V^-_{2n} &= d^{+*}_{2n} e^{(\gamma_{2n}+\gamma_{2n+1})/2}/\Xi_{2n+1}, \\ V^+_{2n} &= -\sigma_{2n}\sigma_{2n-1} d^{-*}_{2n} e^{-(\gamma_{2n}+\gamma_{2n-1})/2}/\Xi_{2n-1}, \\ V^-_{2n+1} &= d^{+*}_{2n} e^{(\gamma_{2n}+\gamma_{2n+1})/2}/\Xi_{2n}, \\ V^+_{2n-1} &= -\sigma_{2n}\sigma_{2n-1} d^{-*}_{2n} e^{-(\gamma_{2n}+\gamma_{2n-1})/2}/\Xi_{2n}, \end{aligned}$$

where the quantities Ξ_n are defined as

$$\begin{aligned} \Xi_{2n} &= r^{+*}_{2n} e^{\gamma_{2n}} - r^{-*}_{2n} e^{-\gamma_{2n}}, \\ \Xi_{2n-1} &= r^{+*}_{2n-2} e^{\gamma_{2n-1}} - r^{-*}_{2n} e^{-\gamma_{2n-1}}. \end{aligned} \qquad \text{(A2)}$$

In non-resonant junctions, the functions Ξ_n approach $r\xi_n$ since energy dispersion of the reflection amplitude is negligibly small. SGS in non-resonant junctions is caused by zeros of the functions ξ_n[21], and renormalization of these functions in the resonance case, $\xi_n \to \Xi_n$, is the reason of considerable difference of the SGS in resonant junction compared to the SGS in non-resonant junctions. We solve equations (A1) by introducing ratios $S_{2n} = c_{2n}/f_{2n-1}$ and $S_{2n+1} = f_{2n+1}/c_{2n}$ and expressing f_n through c_0,

$$f_n = \prod_{i=0}^{n} S_i c_0, \qquad \text{(A3)}$$

c_0 being related to $S_{\pm 1}$ by virtue of the first equation in Eq. (A1). By introducing chain-fractions Z_n,

$$Z_0 = 1 - (d_0^{+*})^2 \frac{e^{\gamma+\gamma_1}}{\Xi_0 \Xi_1 Z_1} - (d_0^{-*})^2 \frac{e^{-\gamma-\gamma_{-1}}}{\Xi_0 \Xi_{-1} Z_{-1}}, \quad \text{(A4)}$$

$$Z_{2n} = 1 - (d_{2n}^{-*})^2 \frac{e^{-\gamma_{2n}-\gamma_{2n-1}}}{\Xi_{2n}\Xi_{2n-1}Z_{2n-1}},$$
$$Z_{2n-1} = 1 - (d_{2n-2}^{+*})^2 \frac{e^{\gamma_{2n-1}+\gamma_{2n-2}}}{\Xi_{2n-1}\Xi_{2n-2}Z_{2n-2}},$$

one can rewrite Eq. (A3) for f_n, e.g. with negative sideband index $n = -2k-1 < 0$, in the following form

$$f_{-2k-1} = \frac{2\xi}{\Delta}(-1)^k d_0^{-*} e^{-(\gamma+\gamma_{-2k-1})/2} \prod_0^{2k+1} \frac{\sigma_{-i}}{\Xi_{-i} Z_{-i}} \prod_1^k d_{-2i}^{+*} d_{-2i}^{-*}. \quad \text{(A5)}$$

An equation for b_{-2k-1} follows from Eqs. (11) and (A5),

$$b_{-2k-1} = r_{-2k-2}^{+*} e^{\gamma_{-2k-1}} \left(1 + \frac{D_{-2k-2}^{+} e^{\gamma_{-2k-2}}}{r_{-2k-2}^{+} \Xi_{-2k-2} Z_{-2k-2}}\right) f_{-2k-1}, \quad \text{(A6)}$$

where $D_n^{\pm} = |d_n^{\pm}|^2$.

Collecting the normal and Andreev transmission amplitudes in Eqs. (A5) and (A6) and substituting them into Eq. (15) for the current, we finally get

$$K_n = -|f_n|^2 \cosh(Re\gamma_n) \left(1 - e^{2Re\gamma_n}(1 - D_{n-1}^{+}) \left|1 + \frac{D_{n-1}^{+} e^{\gamma_{n-1}}}{r_{n-1}^{+} \Xi_{n-1} Z_{n-1}}\right|^2\right), \; n < 0. \quad \text{(A7)}$$

The corresponding equation for positive $n > 0$ is obtained from Eq. (A7) via the substitutions $\gamma \to -\gamma$, $D^+ \to D^-$, and $n-1 \to n+1$.

APPENDIX B: TRANSFORMATION OF K_N

Equation (A7) is not convenient for analysis of the subharmonic gap structure[21]. The current structures are caused by the processes of creation of real excitations during across-the-gap transitions $E \to E_n < -\Delta$. The currents of other side-bands ($E_n > \Delta$) perfectly cancel each other at zero temperature[24]. Furthermore, there is rigorous balance between Andreev and normal channel currents among the states lying within the superconducting gap[24], which provides successive drops of the current with decreasing applied voltage. All of these features are not explicitly seen in the currents K_n in Eq. (A7). Moreover, the current structures related to the creation of real excitations in even-order sidebands are hidden in Eq. (17) which consists of contributions from only odd sidebands.

To overcome this difficulty, we will transform the sideband currents in Eq. (A7) following the method suggested in Ref.[21]. Assuming the transparency D_{n-1}^{+} in Eq. (A7) to be small, we find that the current K_n to leading order is proportional to $\sinh(Re\gamma_n) \sim \theta(E_n^2 - \Delta^2)$. This observation will allow us later [in Eq. (19)] to separate the contributions from states below, $E_n < -\Delta$, and above, $E_n > -\Delta$ the energy gap. Having separated out the leading term, we rewrite Eq. (A7) in the form

$$K_n = |f_n|^2 \cosh(Re\gamma_n) \left(2\sinh(Re\gamma_n) e^{Re\gamma_n} - \frac{D_{n-1}^{+} e^{2Re\gamma_n}}{|\Xi_{n-1} Z_{n-1}|^2} F_{n-1}\right), \quad \text{(B1)}$$

$$F_n = |\Xi_n Z_n|^2 - 2Re\left(e^{\gamma_n^*} r_n^{+} \Xi_n Z_n\right) - D_n^{+} e^{2Re\gamma_n}. \quad \text{(B2)}$$

Equation (B2) possesses a similar property: it is proportional to $\theta(E_n^2 - \Delta^2)$ to leading order with respect to D. Separating out this leading term, we further transform Eq. (B2) into the equation

$$F_n = -2\sinh(2Re\gamma_n) - \frac{D_n^{-} e^{-2Re\gamma_n}}{|\Xi_{n-1} Z_{n-1}|^2} G_{n-1}, \quad \text{(B3)}$$

where

$$G_{n-1} = |\Xi_{n-1} Z_{n-1}|^2 + 2Re\left(e^{-\gamma_{n-1}^*} r_n^{-} \Xi_{n-1} Z_{n-1}\right) - D_n^{-} e^{-2Re\gamma_{n-1}}. \quad \text{(B4)}$$

One more transformation,

$$G_{n-1} = 2\sinh(2Re\gamma_{n-1}) - \frac{D_{n-2}^{+} e^{2Re\gamma_{n-1}}}{|\Xi_{n-2} Z_{n-2}|^2} F_{n-2}, \quad \text{(B5)}$$

accomplishes the cycle, yielding the quantity F in Eq. (B2) with shifted index. Performing repeatedly such transformations, we get for the current in Eq. (A7) the following expansion

$$\begin{aligned} K_n = {} & \theta(E_n^2 - \Delta^2) Q_n + \\ & + 2\theta(E_{n-1}^2 - \Delta^2) e^{-Re\gamma_n} \cosh(Re\gamma_n) Q_{n-1} + \\ & + 2\theta(E_{n-2}^2 - \Delta^2) e^{-Re\gamma_n + 2Re\gamma_{n-1}} \cosh(Re\gamma_n) Q_{n-2} + \\ & + 2\theta(E_{n-3}^2 - \Delta^2) e^{-Re\gamma_n + 2Re\gamma_{n-1} - 2Re\gamma_{n-2}} \cosh(Re\gamma_n) Q_{n-3} + \\ & + \ldots \end{aligned} \quad \text{(B6)}$$

In this equation, the quantity Q_n is defined as

$$Q_n = \frac{8\xi^2 \xi_n |E_n| e^{-\gamma}}{\Delta^4 P_n} D_0^{-} \left(\prod_{i=1}^{k-1} D_{-2i}^{+} D_{-2i}^{-}\right) D_{-2k}^{+} \cdot \cdot \begin{cases} 1, & |n| = 2k \\ D_{-2k}^{-}, & |n| = 2k+1 \end{cases}, \quad \text{(B7)}$$

where

$$P_n = \prod_{i=0}^{|n|} |\Xi_{-i} Z_{-i}|^2. \quad \text{(B8)}$$

Collecting together all terms with similar θ-functions, we can finally rearrange the sum in Eq. (18):

$$\sum_{n=odd} K_n \;\rightarrow\; \sum_{n=1}^{\infty} \tilde{K}_n,\; \tilde{K}_n = \theta(E_n^2 - \Delta^2) Q_n \varphi_n, \quad \text{(B9)}$$

where φ_n is given by the recurrence equation

$$\varphi_{n-1} = 1 + \exp[(-1)^{n+1} 2Re(\gamma_n)]\varphi_n, \;\; \varphi_{-1} = 1.$$

Far from resonance, the quantity P_n may cause strong singularity in the sideband current due to the presence of zeros in the functions Ξ_n, and accounting for the factors Z_n is absolutely necessary for regularization of the singularity[21]. In the resonant case, the functions Ξ_n do not turn to zero because of strong electron-hole dephasing, $r_n^+ \neq r_n^-$, and the quantities Z_n can be omitted from Eq. (B8) in the limit of narrow resonance $\Gamma \ll \Delta$,

$$P_n \approx \prod_{i=0}^{n\;\prime} |\Xi_{-i}|^2 \quad \text{(B10)}$$

The role of Z_n in this limit reduces to cancellation of the terms in the product (B10) which are proportional to the squared resonance amplitudes $(d_n^{\pm})^2$; this is denoted by the prime in Eq. (B10). The presence of the resonant denominators in equation (A2) for Ξ gives rise to renormalization of the normal electron transmission coefficients $D_n^{\pm}$ in Eq. (19) for the current.

[1] L.G. Aslamazov and V.M. Fistul', Sov. Phys. JETP **56**, 655 (1982).
[2] A.T. Tartakovsky and V.M. Fistul', Sov. Phys. JETP **67**, 1695 (1988).
[3] L.I. Glazman and K.A. Matveev, JETP Lett. **49**, 659 (1989).
[4] L.A. Devyatov and M. Yu. Kupriyanov, JETP Lett. **59**, 200 (1994).
[5] I.L. Aleiner, Penny Clarke, and L.I. Glazman, Phys. Rev. B **53**, R7630 (1996).
[6] A. Golub, Phys. Rev. B **52**, 7458 (1995).
[7] A. Frydman and Z. Ovadyahu, Phys. Rev. B **55**, 9047 (1997).
[8] J. Harlbritter, Phys. Rev. B **46**, 11238 (1992).
[9] L.G. Aslamazov and V.M. Fistul', Sov. Phys. JETP **54**, 206 (1981).
[10] I.F. Itskovich and R.I. Shekhter, Sov. J. Low Temp. Phys. **7**, 418 (1981).
[11] H. Takayanagi, T. Akazaki, and J. Nitta, Phys. Rev. Lett. **75**, 3533 (1995).
[12] A. Yacobi, M. Heiblum, D. Mahalu, and H. Shtrikman, Phys. Rev. Lett. **74**, 4047 (1995).
[13] D.C. Ralph, C.T. Black, and M. Tinkham, Phys. Rev. Lett. **74**, 3241 (1995).
[14] S.J. Tans et al., Nature **386**, 474 (1997).
[15] M. Bockrath et al., Science, **275**, 1922 (1997).
[16] P.I. Arseyev and B.A. Volkov, Solid State Comm. **78**, 373 (1991).
[17] C.W.J. Beenakker and H. van Houten, in *Single Electron Tunneling and Mesoscopic Devices* (Springer, Berlin, 1991).
[18] A. Chrestin, T. Matsuyama, and V. Merkt, Phys. Rev. B **49**, 498 (1994).
[19] G. Wendin and V.S. Shumeiko, Superlattices Microstruct. **20**, 569 (1996).
[20] E.N. Bratus', V.S. Shumeiko, and G. Wendin, Phys. Rev. Lett. **74**, 2110 (1995).
[21] V.S. Shumeiko, E.N. Bratus', and G. Wendin, Low Temp. Phys. **23**, 249 (1997).
[22] D. Averin and A. Bardas, Phys. Rev. Lett. **75**, 1831 (1995).
[23] J.C. Cuevas, A. Martin-Rodero, and A. Levy Yeyati, Phys. Rev. B **54**, 7366 (1996).
[24] E.N. Bratus', V.S. Shumeiko, E.V. Bezuglyi, and G. Wendin, Phys.Rev. B **55**, 12666 (1997).
[25] N. van der Post, E.T. Peters, I.K. Yanson, and J.M. van Ruitenbeek, Phys. Rev. Lett. **73**, 2611 (1994).
[26] E. Scheer, P. Joyez, M.H. Devoret, D. Esteve, and C. Urbina, Phys. Rev. Lett. **78**, 3535 (1997).
[27] G. Johansson, E. Bratus', V.S. Shumeiko, and G. Wendin, Physica C **293**, 77 (1997).
[28] A. Levy Yeyati, J.C. Cuevas, A. Lopez-Davalos, and A. Martin-Rodero, Phys. Rev. B **55**, R6317 (1997).
[29] R. Landauer, IBM J. Res. Dev. **1**, 223 (1957).
[30] M.A. Büttiker, Phys. Rev. Lett. **57**, 1761 (1986).
[31] Y. Imry, in *Directions in Condensed Matter Physics* (World Scientific, Singapore, 1986) p. 102.
[32] Definition of long SIS junctions was introduced in G. Wendin and V.S. Shumeiko, Phys. Rev. B **53**, R6006 (1996).
[33] C. Dekker, Private communication.
[34] Yu. V. Nazarov, Physica B **189**, 57 (1883).
[35] N.C. van der Vaart et al. Phys. Rev. Lett. **74**, 4702 (1995).
[36] T.M. Klapwijk, G.E. Blonder, and M. Tinkham, Physica B+C **109-110**, 1657 (1982).
[37] R. Kleiner and P. Müller, Phys. Rev. B **49**, 1327 (1994).

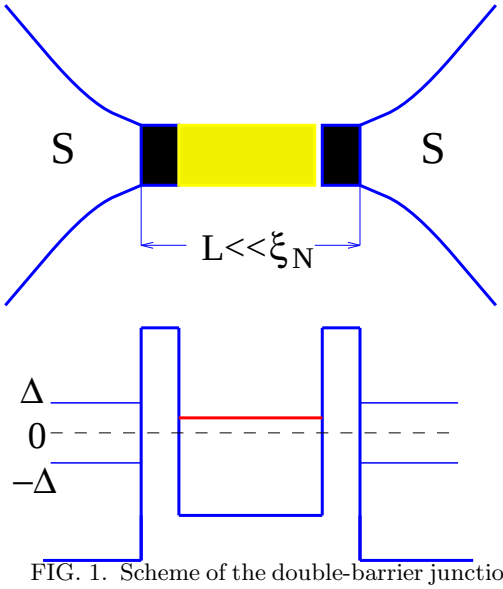

FIG. 1. Scheme of the double-barrier junction. Upper part: dark regions - tunnel barriers; shadowed region - normal conductor. Lower part: energy diagram showing one normal resonant level inside the superconducting gap.

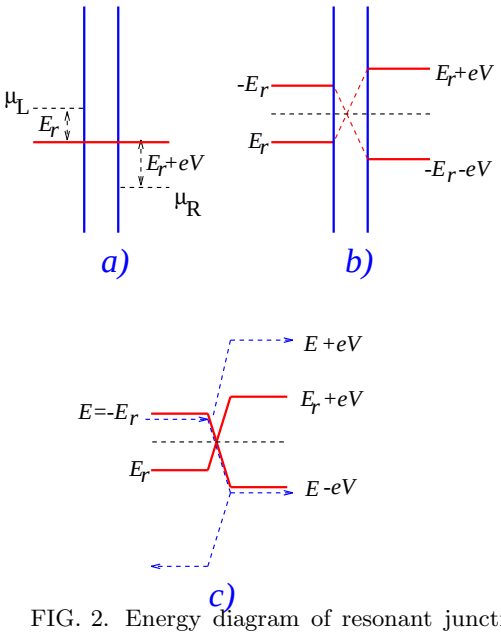

FIG. 2. Energy diagram of resonant junctions under applied voltage. a) Resonance in normal junction; the distance to the chemical potentials of the left and right electrodes is E_r and $E_r + eV$ respectively. b) Electron and hole resonances in superconducting junction; the resonance offset is different in the left and right electrodes with respect to the global chemical potential after equalizing the chemical potentials of the electrodes by means of the gauge transformation. c) Resonant transition in the scattering diagram.

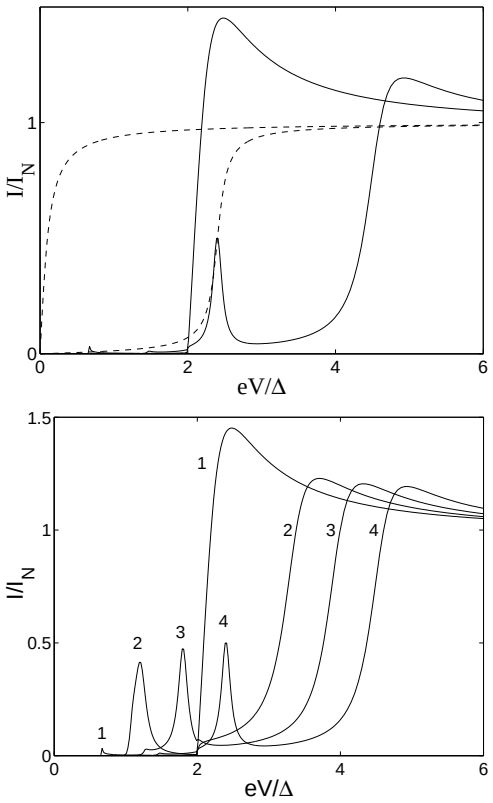

FIG. 3. IVC of symmetric resonant junctions. a) IVC of normal junction (dashed line) and superconducting junction (solid line), $E_0/\Delta = 0$, 1.2 (left and right curves respectively), $\Gamma/\Delta = 0.05$. b) IVC of superconducting junction, $E_0/\Delta = 0$. (1), 0.6 (2), 0.9 (3), 1.2 (4).

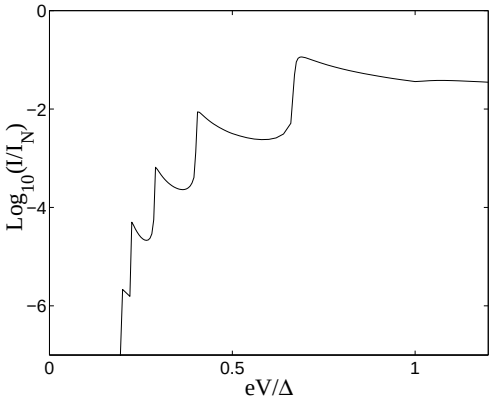

FIG. 4. Subharmonic gap structure on IVC of symmetric resonant junction, $E_0 = 0$, $\Gamma/\Delta = 0.2$. The structures appear only at $eV = 2\Delta/n$ with odd n.

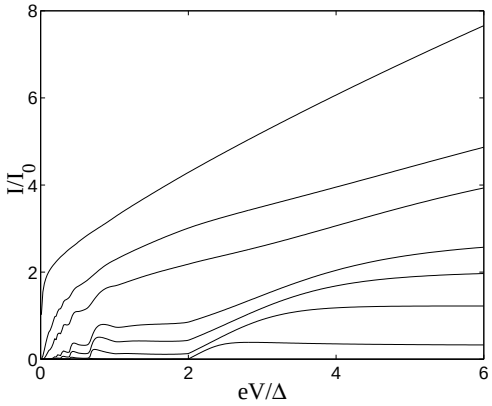

FIG. 5. IVC of symmetric resonant junctions with $E_0 = 0$ and $\Gamma/\Delta \in \{0.1, 0.4, 0.7, 1.0, 2.0, 3.0, 10.0\}$ (from bottom to top). The current is normalized by $I_0 = e\Delta/\hbar\pi$.

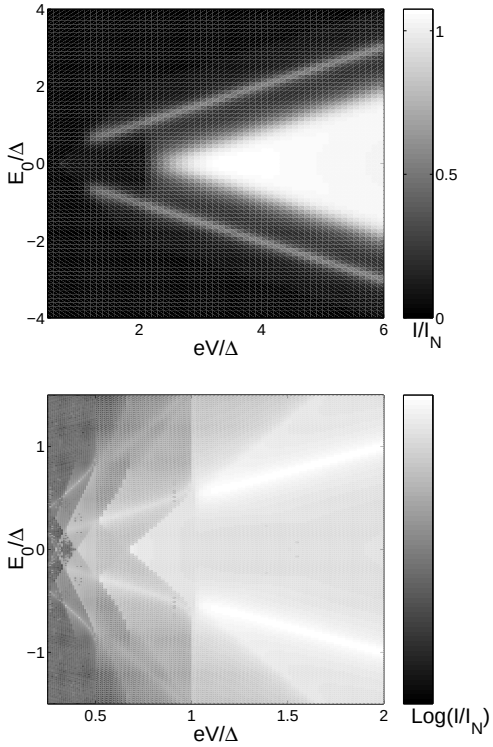

FIG. 6. Intensity plots showing the dependence of the current $I(V, E_0)$ on the applied bias voltage V and the resonance position E_0. (a) Single-particle current and pair current at $eV > \Delta$ ($\Gamma = 0.2\Delta$). (b) Pair current and high-order currents at $eV < 2\Delta$ ($\Gamma = 0.05\Delta$).

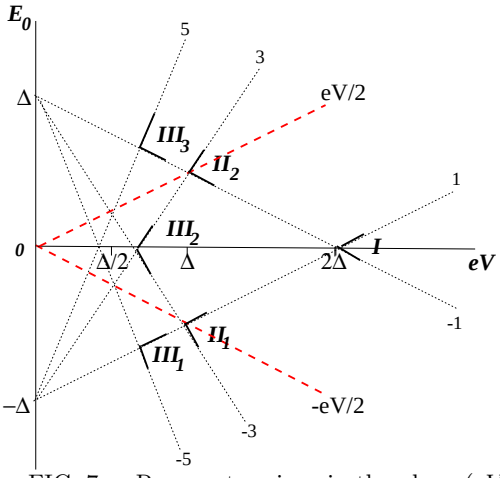

FIG. 7. . Resonant regions in the plane $(eV, E_0,)$ for sideband currents I_n. I, II and III are resonant regions for single-particle current, pair current and three-particle current respectively. The resonant regions are bound by dotted lines $E_0 = \pm(\Delta - neV/2)$ (labeled with $\pm n$). Bold dashed lines show positions of double resonances.

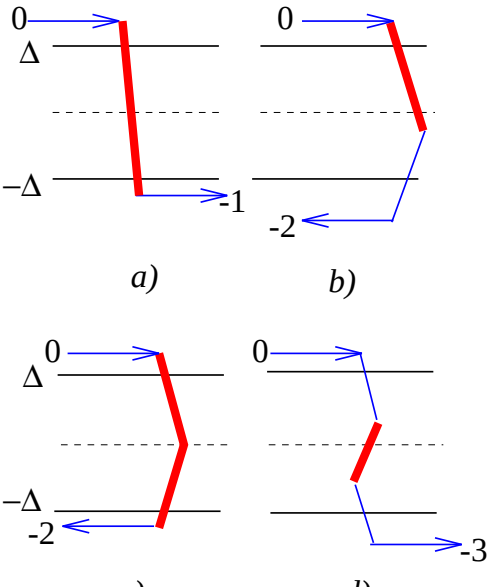

FIG. 8. Resonant scattering diagrams; bold lines show resonant transitions. a) Resonance in single-particle current; b) single resonance in the pair current; c) double resonance in the pair current; d) central resonance in the three-particle current.

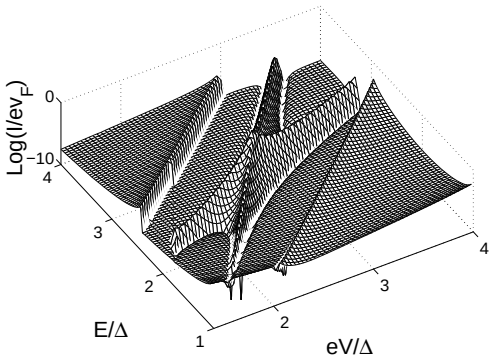

FIG. 9. Spectral density of the pair current as a function of bias voltage for $\Gamma/\Delta = 0.05$. The current peak appears at the crossing point of two single resonances.

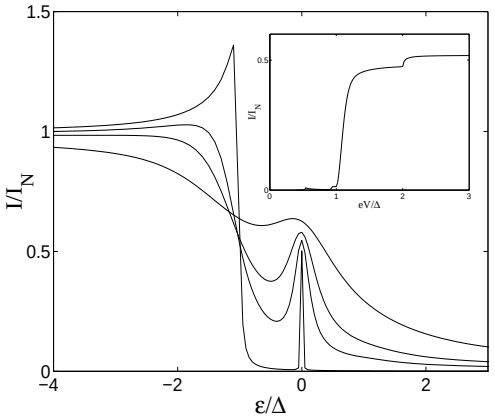

FIG. 10. Current for asymmetric junction at large voltage ($eV = 1000\Delta$ as a function of the position of the resonance $\epsilon = |E_0| - eV/2$ for different resonance width $\Gamma/\Delta \in \{0.01, 0.21, 0.41, 0.61, 0.81, 1.01\}$ (from top to bottom at the left side of the figure). Inset shows IVC for $\epsilon = 0$: the resonance level coincides with the chemical potential of one of the electrodes.